

Characterization of cathode-electrolyte interface in all-solid-state batteries using TOF-SIMS, XPS, and UPS/LEIPS

Cite as: *J. Vac. Sci. Technol. B* **39**, 044001 (2021); doi: [10.1116/6.0001044](https://doi.org/10.1116/6.0001044)

Submitted: 23 March 2021 · Accepted: 3 May 2021 ·

Published Online: 24 May 2021



[View Online](#)



[Export Citation](#)



[CrossMark](#)

Shin-ichi Iida,^{1,a)} Masahiro Terashima,¹ Kazutoshi Mamiya,¹ Hsun-Yun Chang,¹ Shunsuke Sasaki,² Atsuo Ono,² Takahito Kimoto,² and Takuya Miyayama¹

AFFILIATIONS

¹ULVAC-PHI, Inc., 2500 Hagisono, Chigasaki, Kanagawa 253-8522, Japan

²ULVAC Inc., 2500 Hagisono, Chigasaki, Kanagawa 253-8543, Japan

^{a)}Electronic mail: shinichi_iida@ulvac.com

ABSTRACT

In recent years, all-solid-state batteries (ASSBs) have been attracting attention as the next generation batteries for electric vehicles, energy storage systems, etc. Despite the growing interest, there are still many challenges faced in the commercial use of ASSBs. One of the biggest issues is the internal resistance, especially generated at the interface between solid electrolyte and electrode. The internal resistance at the interface limits the charge-discharge cycling performances. In order to solve this issue, it is necessary to examine the chemical and physical interactions at the interface. In this study, we have performed a detailed characterization of a LiPON/LiCoO₂ interface using time-of-flight secondary ion mass spectrometry, x-ray photoelectron spectroscopy, ultraviolet photoelectron spectroscopy, and low-energy inverse photoelectron spectroscopy to obtain information on chemical species, chemical compositions, chemical states, and energy band diagrams. These powerful techniques have revealed that an interlayer between LiPON and LiCoO₂ was formed due to the temperature rise during the manufacturing process. The temperature rise caused a change of the LiPON network structure and stimulated Co reduction in the LiCoO₂ layer near the interface. Energy band diagram analysis suggests that the electron diffusion from LiPON to LiCoO₂ may have triggered the reduction of Co. We concluded that the chemical changes that occur at the interface caused an increase in interfacial impedance. Preventing the chemical reduction of Co would be a key to minimize the internal resistance. In this article, the detailed chemical interactions between the LiPON and LiCoO₂ layers will be discussed.

Published under an exclusive license by the AVS. <https://doi.org/10.1116/6.0001044>

I. INTRODUCTION

Rechargeable lithium-ion batteries (LIBs) are widely used in most mobile electronic devices such as laptops, smartphones, etc. LIBs have been indispensable in our modern society. However, using existing LIB technology in electric vehicle (EV) or plug-in hybrid electric vehicle (PHEV) applications brings about a critical safety issue because current, commercially available LIBs contain combustible organic liquid electrolytes. Furthermore, because organics in the electrolytes are very vulnerable to high temperatures, the problem of thermal stability has also arisen. All-solid-state batteries (ASSBs), in which all components including electrolytes are solid, have recognizable safety and thermal stability advantages, thus making them a feasible solution for these applications. Moreover, ASSBs are also significant contributors to

microdevice applications, such as smart-cards, medical implants, and wireless sensors, which have become increasingly more important technologies in recent years. For such reasons, the commercialization of ASSBs is highly anticipated not only for large-scale energy storage devices but also microdevices.^{1–3} However, the internal resistance generated at the interface between the solid electrolyte (SE) and an electrode is one of the biggest obstacles for the practical use of ASSBs. This internal resistance restricts the high-speed transport of Li ions during charging/discharging cycles. In other words, the functionality of ASSBs strongly depends on the properties at the SE/electrode interface. In order to reduce the internal resistance, various types of surface modifications between SE and cathode have been reported^{4–6} with subsequent Li ion transport significantly improved upon charge/discharge cycles.

Although numerous studies on the SE/electrode interface of ASSBs have been conducted, the mechanism of increasing the interfacial impedance is still unclear.⁷ Therefore, further investigation on the interactions between the SE and the electrode is required.

X-ray photoelectron spectroscopy (XPS) and time-of-flight secondary ion mass spectrometry (TOF-SIMS) are commonly used to characterize the chemical properties at the SE/cathode interface. In addition to the chemical properties determined by XPS and TOF-SIMS, information on energy levels of cathodes and SEs is necessary for understanding the behavior at the interface because the chemical reactions are greatly affected by their electrical characteristics. Ultraviolet photoelectron spectroscopy (UPS) is a suitable analytical method for determining the ionization potential (IP) and valence band maximum (VBM) position with low sample damage. However, obtaining an electron affinity (EA) and conduction band minimum (CBM) position is challenging. SEs such as lithium phosphorous oxy-nitride (LiPON) is often sensitive to electron beam irradiation. Sample damage induced by the high-energy electron beam in scanning transmission electron microscopy (STEM), or electron energy loss spectroscopy (EELS), has been reported.^{8–10} For this reason, conventional high-energy inverse photoelectron spectroscopy (IPES) can cause significant damage to such samples. In contrast, low-energy inverse photoelectron spectroscopy (LEIPS) having a low-energy electron beam (<5 eV) is an effective method to evaluate the energy band status for the materials that are sensitive to electron beam irradiation.^{11–14} The energy diagram obtained by UPS/LEIPS enables us to predict the chemical state and chemical reaction of the SE/cathode interface.

In this study, the combination of TOF-SIMS, XPS, and UPS/LEIPS was applied to characterize the interface between the LiCoO₂ cathode and LiPON electrolyte to obtain information on chemical species, compositions, chemical bonding states, and energy band diagrams.

II. EXPERIMENT

A. Sample preparation

In this study, a thin-film ASSB sample composed of a metal lithium anode, LiCoO₂ cathode, and LiPON electrolyte was used. LiCoO₂ is a commonly used positive electrode, and the chemical stability of LiPON makes it widely used as an oxide-based solid electrolyte.^{15,16} A Pt/Ti layer was coated on the glass as a cathode current collector (CCC), and LiCoO₂ was deposited on the CCC surface using a radio frequency (RF) superimposed direct-current (DC) sputtering. LiCoO₂ was annealed at 500 °C in air for 10 h for crystallization. The LiPON film was prepared by RF sputtering at a power of 2 kW in a nitrogen atmosphere of 0.3 Pa using a Li₃PO₄ target having a deposition rate of ~15 nm/min. These manufacturing processes were carried out using a multisputtering system (SME-200J, ULVAC Inc., Japan). The distance between the target and substrate was 120 mm, and the maximum temperature during LiPON deposition was recorded by temperature label (TEM-PLATE, Palmer Wahl instruments, Inc.) attached to the substrate. Although the cooling system was equipped under the substrate, the temperature was 200 °C within the 2-h deposition. Finally, the battery device was completed by coating the metal Li anode, anode current collector, and a protective layer. In a previous study, the result of the

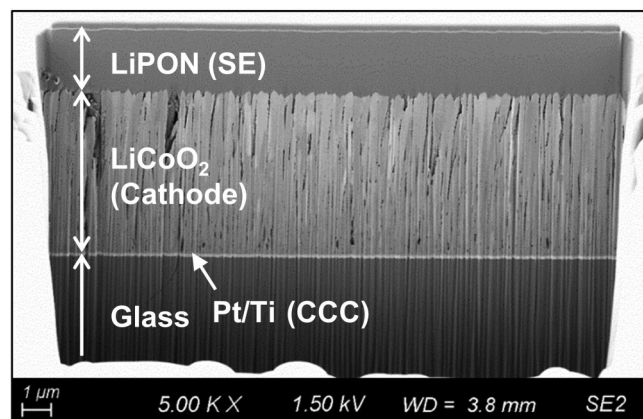


FIG. 1. Cross-sectional SEM image from an ASSB sample prepared by FIB. LiPON, LiCoO₂, CCC, and glass substrate were clearly identified.

electrochemical impedance spectroscopy (EIS) measurement suggested that this device had an internal resistance at the LiPON/LiCoO₂ interface.¹⁷

Figure 1 shows a cross-sectional scanning electron microscopy (SEM) image from a thin-film ASSB sample prepared by focused ion beam (SMI-2050, Seiko Instruments Inc., Japan). The FIB milling and polishing, using 30 keV Ga⁺, was done with 5 nA for 20 min and 1 nA for 10 min, respectively. In this study, a fresh thin-film ASSB sample (no charge/discharge cycles, prior to deposition of a Li anode) was used. The SEM image clearly identified the individual layers. It was found that the thicknesses of the LiPON and LiCoO₂ layers were 2.2 and 5.7 μm, respectively. An examination of the LiPON/LiCoO₂ sample was performed using TOF-SIMS, XPS, and UPS/LEIPS.

B. Measurement conditions

Table I summarizes the detailed experimental conditions for TOF-SIMS, XPS, and UPS/LEIPS. TOF-SIMS depth profiles were acquired using a PHI nanoTOF II (ULVAC-PHI Inc., Japan) equipped with a Bi cluster ion gun for analysis and an Ar ion gun for sputtering. TOF-SIMS acquisition was performed using Bi₃⁺ with the data collected in the positive ion polarity (+SIMS). The base chamber pressure was less than 1×10^{-7} Pa. Mass calibration of the TOF-SIMS spectrum was done with Li⁺, Li₂O⁺, and Li₃O⁺. Data acquisition and data processing were accomplished using the SMARTSOFT-TOF and TOF-DR software (ULVAC-PHI Inc., Japan), respectively.

XPS and UPS/LEIPS measurements were performed using a PHI VersaProbe III (ULVAC-PHI Inc., Japan), which is a multitechnique system that allows us to conduct *in situ* XPS and UPS/LEIPS analysis and sample heating while at the same position on a sample. The vacuum pressure in the chamber was maintained at $\sim 10^{-8}$ Pa. Details of the multitechnique system and data acquisition using UPS and LEIPS are described in Ref. 14.

TABLE I. Summary of measurement conditions.

| TOF-SIMS | | |
|------------|----------|------------------------------------------------------------------------------------------------------------------------------|
| Sputtering | Analysis | Ion species Energy Ion current Raster size |
| | | Bi ₃ ⁺⁺ 60 keV 3.6 nA (DC) 50 × 50 μm ² |
| | | Charge neutralization |
| | | Ion species Energy Ion current Raster size |
| | | Ar ⁺ 15 eV e ⁻ 2 keV 800 nA 300 × 300 μm ² |
| | XPS | |
| UPS | Analysis | X-ray Energy Raster size Pass energy Energy step Charge neutralization |
| | | AlK α 1486.6 eV 100 × 100 μm ² 69 eV 0.125 eV 1 eV e ⁻ and 10 eV Ar ⁺ |
| | LEIPS | |
| | Analysis | UV source Energy Pass energy Energy step |
| | | He I 21.2 eV 1.3 eV 0.02 eV |
| | LEIPS | |
| XPS | Analysis | Electron energy Bandpass filter Energy step |
| | | 0–5 eV 3.7 eV 0.04 eV |
| | | |

The XPS data were collected using Al K α radiation (1486.6 eV) with a pass energy of 69 eV, and the binding energy of the XPS spectra was calibrated using Co 2p_{3/2} from LiCoO₂ at 780.0 eV.¹⁸ The energy band diagram analysis was performed in combination with UPS/LEIPS. The He I line (21.2 eV) with a pass energy of 1.3 eV was used for UPS measurement. For the LEIPS measurements, the spectra were acquired using the electron beam with energies less than 5 eV, and the near-ultraviolet light emitted from the sample surface was detected with a photomultiplier through a bandpass filter. For XPS and UPS/LEIPS, spectra acquisition and data processing were carried out using the SMARTSOFT-VP and MULTIPAK software (ULVAC-PHI Inc., Japan), respectively.

III. RESULTS AND DISCUSSION

A. TOF-SIMS depth profiling of the LiPON/LiCoO₂ sample

Figure 2 shows the TOF-SIMS depth profile from the LiPON surface to the glass substrate. In this study, the sputtering rate was determined from the time to remove individual layers. The Li₄PO₄⁺ ion is one of the main peaks of LiPON and is considered to be Li⁺ adduct with Li₃PO₄. No significant peaks containing nitrogen were

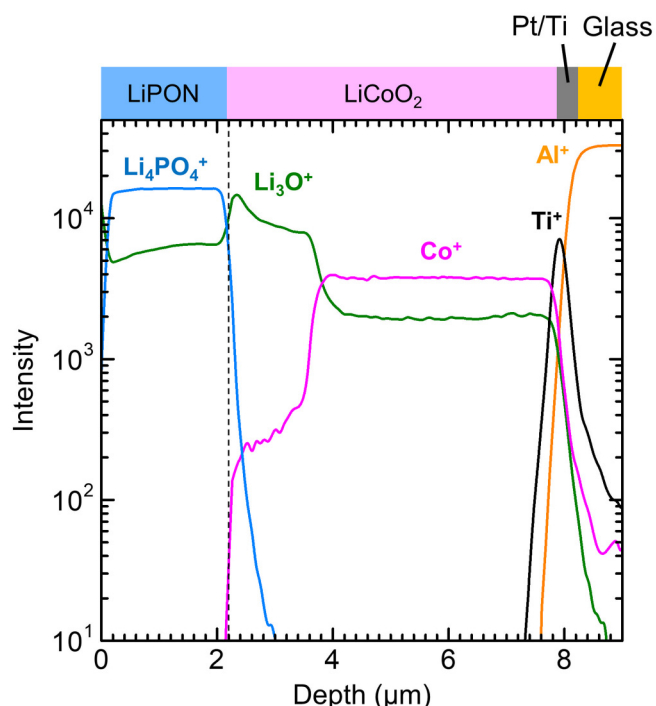


FIG. 2. TOF-SIMS depth profile of the ASSB sample from the LiPON surface to the glass substrate. Bifurcation was observed in the LiCoO₂ layer.

observed. In the LiCoO₂ layer, the Co⁺ intensity was observed to be stepwise and the layer was able to be divided into two regions. The positive ion spectra extracted from (a) LiPON, (b) low, and (c) high Co⁺ intensity regions were shown in Fig. 3, respectively. In the region where the Co⁺ intensity was low, Li₃O⁺ was relatively high. In particular, Li₃O⁺ was localized in the LiCoO₂ layer near the interface. The result suggested that there was an interlayer with a specific chemical state near the LiPON/LiCoO₂ interface. Interestingly, no distinct interlayer was observed from the 100 nm-thick LiPON/LiCoO₂ interface (Fig. 4).

Despite the very unique behavior observed at the 2.2 μm-thick LiPON/LiCoO₂ interface, it was not observed at the 100 nm-thick LiPON/LiCoO₂ sample. Next, the effect of the difference in the thickness of the LiPON film on the chemical property of the interface was investigated.

B. Chemical properties at the initial stage of LiPON deposition

A 100 nm-thick LiPON/LiCoO₂ sample was heated in the XPS chamber using the sample heating holder. The temperature of the sample holder was controlled to be maintained at 200 °C for 2 h. This heating condition mirrors the estimated substrate temperature during the deposition of the 2.2 μm-thick LiPON film. After heating the 100 nm-thick LiPON/LiCoO₂ sample, XPS measurement was performed at room temperature. Figure 5(a) shows the

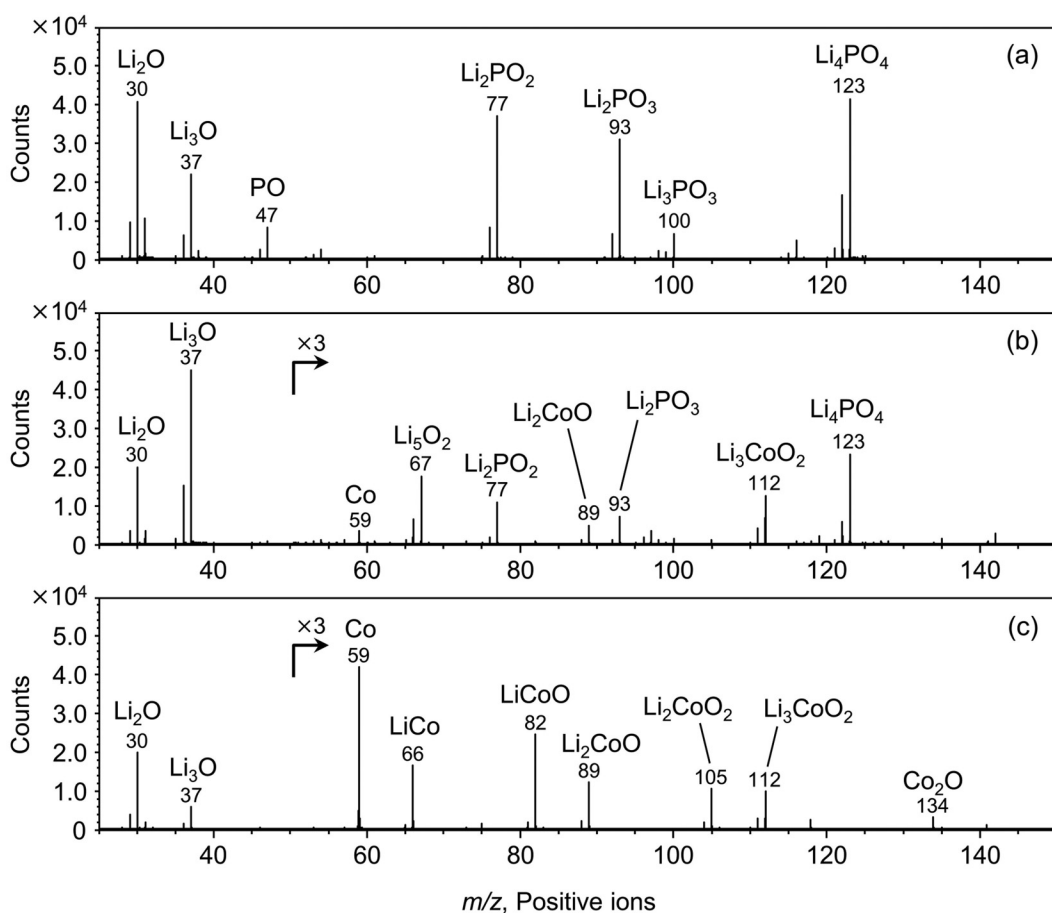


FIG. 3. Positive ion spectra extracted from the depth profile shown in Fig. 2. (a) LiPON, (b) low, and (c) high Co^+ intensity regions.

XPS spectra of Li 1s, N 1s, P 2p, O 1s, and Co 2p_{3/2} from the 100 nm-thick LiPON/LiCoO₂ surface before heating. Multiple reports on the chemical state of LiPON have appeared;^{19–22} O 1s spectra from LiPON were assigned three components attributed to P=O (nonbridging oxygen), Li⁺—O—P (bridging oxygen), and P—O—P (bridging oxygen). N 1s spectra were decomposed into two different bonding states of nitrogen ($-\text{N}=$ and $-\text{N}<$). These components based on the LiPON network structure were observed in this experiment. Although LiCoO₂ was covered with the 100 nm-thick LiPON film, 1.8% Co was detected on the surface because the surface roughness of LiCoO₂ was \sim 100 nm. The TOF-SIMS depth profile also indicated that Co was exposed on the 100 nm-thick LiPON/LiCoO₂ surface (seen in Fig. 4). Before heating, the satellite derived from Co³⁺ was still observed in the Co 2p_{3/2} spectrum, indicating that the chemical state of LiCoO₂ remained after deposition of 100 nm-thick LiPON film. As shown in Fig. 5(b), Co 2p_{3/2} reveals the disappearance of the Co³⁺ satellite and the appearance of metal Co after heating. On the other hand, the chemical state of Co remained Co³⁺ when the same heat

treatment was applied to the LiCoO₂ surface (data not shown). These examinations reveal that some interaction occurs between LiPON and LiCoO₂ during heating.

Table II shows the atomic concentration (%) of Li, N, P, O, and Co obtained from XPS spectra of 100 nm-thick LiPON/LiCoO₂ surface. The concentration ratio of N/P was 0.49 and was nearly unchanged before and after heating, while the O/P ratio increased from 3.5 to 3.8; this suggests the incorporation of oxygen into LiPON. Taking into account the decrease of P—O—P and increase of P=O after heating [see Fig. 5(b)], some of the bridging oxygen was converted into nonbridging oxygen. Meanwhile, oxygen was incorporated from LiCoO₂. As a result, the Co reduction occurred in the LiCoO₂ layer near the interface.

What this detailed chemical analysis reveals is that the difference in chemical properties between 2.2 μm - and 100 nm-thick LiPON is a result of the temperature rise during the manufacturing process. No obvious reaction between LiPON and LiCoO₂ occurred during the 100 nm-thick LiPON deposition because the temperature rise was not enough to induce the interaction. On the other

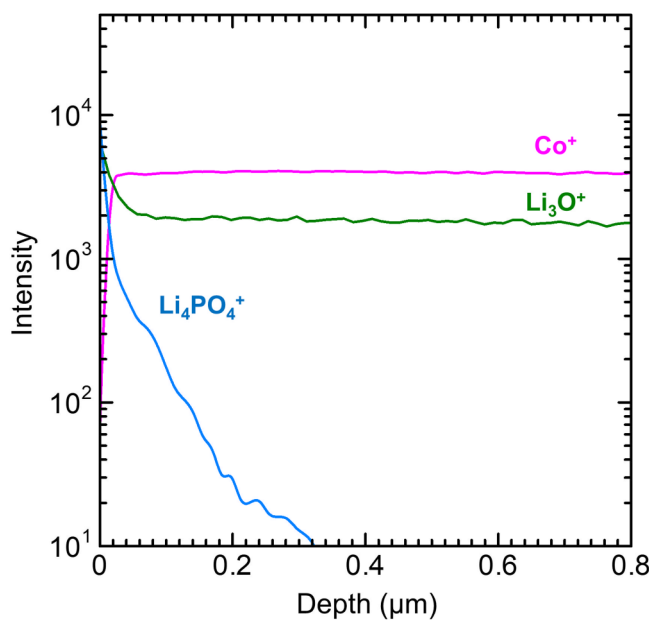


FIG. 4. TOF-SIMS depth profile of the 100 nm-thick LiPON/LiCoO₂ sample. The only difference from 2.2 μm-thick LiPON/LiCoO₂ sample is the deposition time.

hand, with the 2.2 μm-thick LiPON film deposition, the temperature rise altered the LiPON network structure. In the LiPON layer, oxygen was incorporated from LiCoO₂, stimulating the Co reduction from Co³⁺ to Co⁰⁺. It can be concluded that the change in the chemical composition as well as the chemical state at the SE/cathode interface may cause an increase in interfacial resistance.

C. Energy band diagram analysis

The UPS/LEIPS measurements were carried out to examine the energy band diagrams of LiCoO₂ and LiPON surfaces. In this experiment, a single layer of LiCoO₂ and LiPON was deposited on CCC; the thickness of the films was 5.7 μm and 100 nm, respectively. The UPS/LEIPS spectra of LiCoO₂ and LiPON surfaces are shown in Fig. 6. The obtained bandgap from the LiCoO₂ surface was 2.4 eV, which correlated well with the reported experimental bandgap of 2.1–2.7 eV.^{23–25} For LiPON, the bandgap was 5.2 eV and was slightly lower than the theoretical bandgap of ~6.0 eV.^{26,27} Figure 7 shows the schematic diagram of each band structure relative to the vacuum level. The results suggested that the electrons in LiPON diffused into LiCoO₂ at the initial stage of the LiPON deposition on LiCoO₂ because the Fermi level of LiCoO₂ was lower than that of LiPON. It was possible that these electrons triggered the Co reduction. Furthermore, the temperature rise might stimulate the interaction between LiPON and LiCoO₂. As discussed above, the reduction of Co caused the decomposition of

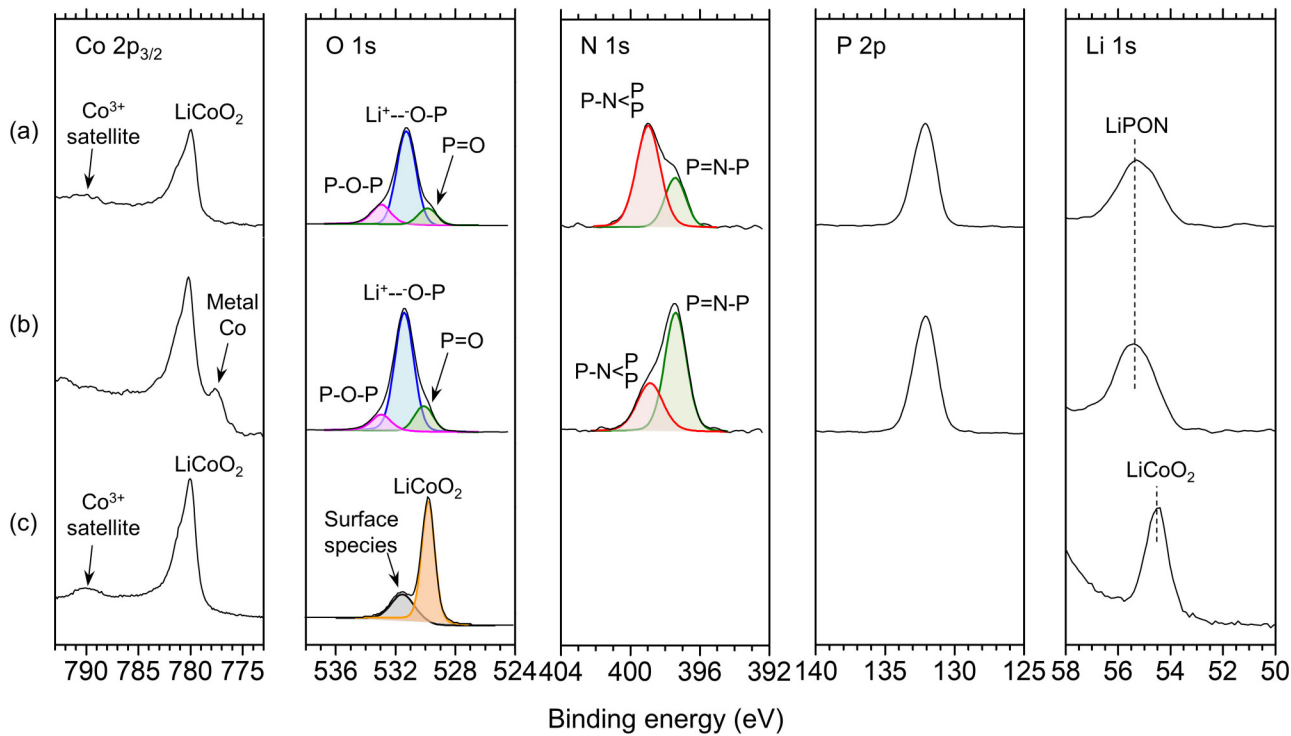


FIG. 5. XPS spectra of Li 1s, N 1s, P 2p, O 1s, and Co 2p_{3/2} from the 100 nm-thick LiPON /LiCoO₂ surface (a) before and (b) after heating. XPS spectra of Li 1s, O 1s, and Co 2p_{3/2} from the LiCoO₂ surface are shown in (c) as a reference.

TABLE II. Atomic concentration of 100 nm-thick LiPON/LiCoO₂ surface before and after heating.

| | Atomic concentration (%) | | | | |
|----------------|--------------------------|------|------|------|-------|
| | Li 1s | P 2p | N 1s | O 1s | Co 2p |
| Before heating | 24 | 15 | 7.3 | 52 | 1.8 |
| After heating | 24 | 14 | 6.9 | 53 | 2.8 |

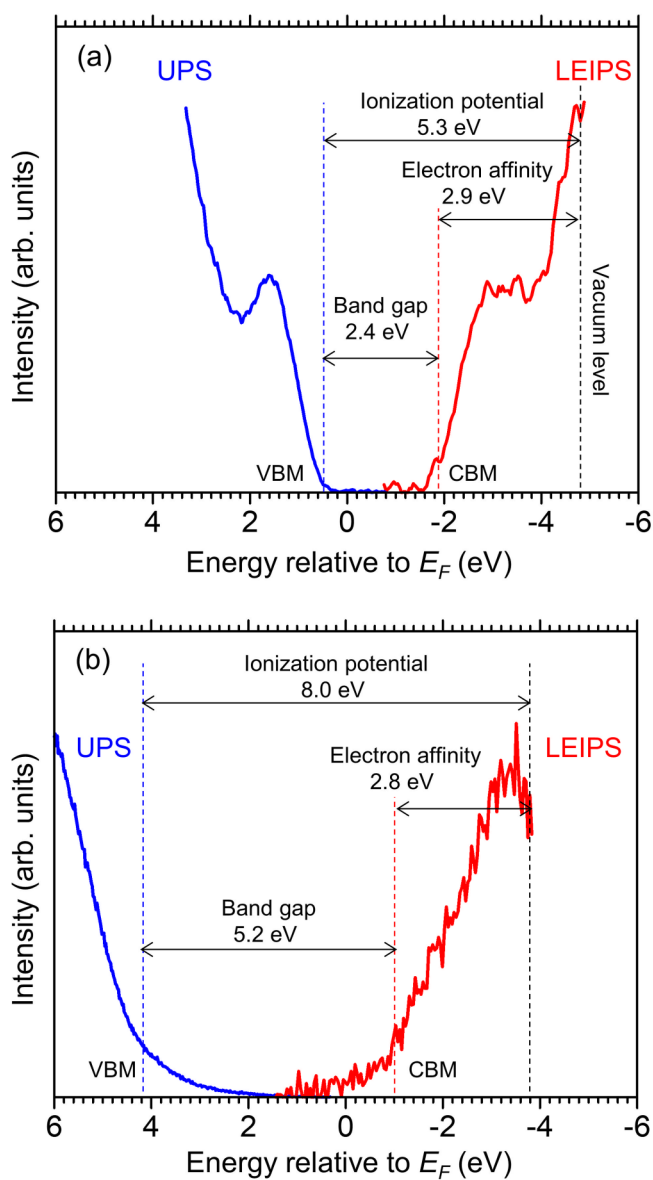


FIG. 6. UPS/LEIPS spectra from (a) LiCoO₂ and (b) LiPON surfaces.

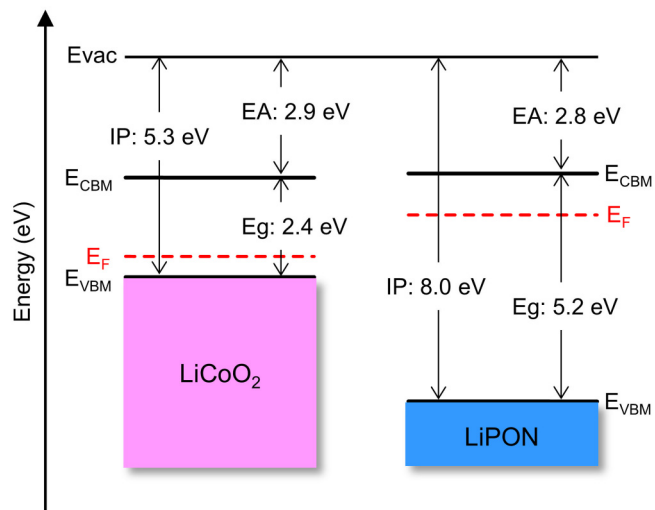


FIG. 7. Energy band diagrams of LiCoO₂ and LiPON surfaces relative to the vacuum level.

LiCoO₂. If the temperature rise can be suppressed during the LiPON deposition (for example, lowering the power of RF sputtering, strengthening the cooling system, or increasing the distance between the target and substrate), it may be possible to prevent the Co reduction.

IV. SUMMARY AND CONCLUSIONS

A detailed characterization of the interface between the SE and cathode was performed using surface analysis techniques such as TOF-SIMS, XPS, and UPS/LEIPS for the investigation of the internal resistance. The results can be summarized as follows:

- (1) The LiCoO₂ layer was bifurcated after the deposition of a 2.2 μm -thick LiPON film.
- (2) It was found that the LiPON network structure was changed due to the temperature rise and LiPON incorporated oxygen from LiCoO₂. The oxygen incorporation stimulated the reduction of Co from Co³⁺ to Co⁰⁺. It might further lead to the decomposition of LiCoO₂.
- (3) The results of the energy band diagram analysis suggest that the electron diffusion from LiPON to LiCoO₂ may have triggered the reduction of Co. Furthermore, the temperature rise likely stimulated the interaction between LiPON and LiCoO₂. Suppressing the Co reduction would be a key factor in minimizing the internal resistance.

TOF-SIMS, XPS, and UPS/LEIPS have been shown to deliver detailed information on ASSBs. Comprehensive surface analysis is a critical method of material evaluation in further understanding the interactions between the SE/electrode as well as improving commercial production methods for better batteries.

DATA AVAILABILITY

The data that support the findings of this study are available from the corresponding author upon reasonable request.

REFERENCES

- ¹A. C. Luntz, J. Voss, and K. Reuter, *J. Phys. Chem. Lett.* **6**, 4599 (2015).
- ²Y. Zhu, J. C. Gonzalez-Rosillo, M. Balaish, Z. D. Hood, K. J. Kim, and J. L. M. Rupp, *Nat. Rev. Mater.* **6**, 313 (2020).
- ³T. Famprikis, P. Canepa, J. A. Dawson, M. S. Islam, and C. Masquelier, *Nat. Mater.* **18**, 1278 (2019).
- ⁴N. Ohta, K. Takada, L. Zhang, R. Ma, M. Osada, and T. Sasaki, *Adv. Mater.* **18**, 2226 (2006).
- ⁵N. Ohta, K. Takada, I. Sakaguchi, L. Zhang, R. Ma, K. Fukuda, M. Osada, and T. Sasaki, *Electrochem. Commun.* **9**, 1486 (2007).
- ⁶K. Kishida, N. Wada, Y. Yamaguchi, H. Inui, M. Demura, Y. Iriyama, and Z. Ogumi, *J. Mater. Res.* **25**, 1583 (2010).
- ⁷J. Janek and W. G. Zeier, *Nat. Energy* **1**, 1 (2016).
- ⁸Z. Wang, D. Santhanagopalan, W. Zhang, F. Wang, H. L. Xin, K. He, J. Li, N. Dudney, and Y. S. Meng, *Nano Lett.* **16**, 3760 (2016).
- ⁹C. Zhang, Y. Feng, Z. Han, S. Gao, M. Wang, and P. Wang, *Adv. Mater.* **32**, 1903747 (2020).
- ¹⁰D. Santhanagopalan, D. Qian, T. McGilvray, Z. Wang, F. Wang, F. Camino, J. Graetz, N. Dudney, and Y. S. Meng, *J. Phys. Chem. Lett.* **5**, 298 (2014).
- ¹¹H. Yoshida, *Rev. Sci. Instrum.* **84**, 103901 (2013).
- ¹²H. Yoshida, *J. Electron Spectrosc. Relat. Phenom.* **204**, 116 (2015).
- ¹³H. Yoshida, *Rev. Sci. Instrum.* **85**, 016101 (2014).
- ¹⁴M. Terashima, T. Miyayama, T. Shirao, H. W. Mo, Y. Hatae, H. Fujimoto, and K. Watanabe, *Surf. Interface Anal.* **52**, 948 (2020).
- ¹⁵J. B. Bates, N. J. Dudney, G. R. Gruzalski, R. A. Zuhar, A. Choudhury, C. F. Luck, and J. D. Robertson, *Solid State Ionics* **53–56**, 647 (1992).
- ¹⁶J. B. Bates, N. J. Dudney, B. Neudecker, A. Ueda, and C. D. Evans, *Solid State Ionics* **135**, 33 (2000).
- ¹⁷S. Sasaki, A. Suzuki, and T. Jimbo, *The 56th Battery Symposium in Japan*, WINC Aichi, Japan, 11–13 November 2015 (Electrochemical Society of Japan, Tokyo, 2015).
- ¹⁸A. Uhart, J. B. Ledet, B. Pecquenard, F. Le Cras, M. Proust, and H. Martinez, *ACS Appl. Mater. Interfaces* **9**, 33238 (2017).
- ¹⁹B. Fleutot, B. Pecquenard, H. Martinez, M. Letellier, and A. Levasseur, *Solid State Ionics* **186**, 29 (2011).
- ²⁰N. Mascaraque, J. L. G. Fierro, A. Durán, and F. Muñoz, *Solid State Ionics* **233**, 73 (2013).
- ²¹S. Jacke, J. Song, G. Cherkashinin, L. Dimesso, and W. Jaegermann, *Ionics* **16**, 769 (2010).
- ²²M. Fingerle, R. Buchheit, S. Sicolo, K. Albe, and R. Hausbrand, *Chem. Mater.* **29**, 7675 (2017).
- ²³K. Kushida and K. Kuriyama, *Solid State Commun.* **123**, 349 (2002).
- ²⁴J. van Elp, J. L. Wieland, H. Eskes, P. Kuiper, G. A. Sawatzky, F. M. F. de Groot, and T. S. Turner, *Phys. Rev. B* **44**, 6090 (1991).
- ²⁵A. Chakraborty, M. Dixit, D. Aurbach, and D. T. Major, *npj Comput. Mater.* **4**, 60 (2018).
- ²⁶K. Senevirathne, C. S. Day, M. D. Gross, A. Lachgar, and N. A. W. Holzwarth, *Solid State Ionics* **233**, 95 (2013).
- ²⁷G. Cherkashinin, Z. Yu, R. Eilhardt, L. Alff, and W. Jaegermann, *Adv. Mater. Interfaces* **7**, 2000276 (2020).